

## Macroscopic theory of pulsed-laser annealing. I. Thermal transport and melting

R. F. Wood

*Solid State Division, Oak Ridge National Laboratory, Oak Ridge, Tennessee 37830*

G. E. Giles

*Computer Sciences Division, Oak Ridge National Laboratory, Oak Ridge, Tennessee 37830*

(Received 18 August 1980)

Pulses of radiation from ruby and Nd:YAG  $Q$ -switched lasers have been used recently to anneal the lattice damage caused by ion implantation of semiconductors. Other similar applications include the laser-induced diffusion of thin dopant films deposited on the surface of samples, recrystallization of doped amorphous films deposited on single-crystal substrates, and the removal of precipitates present after conventional high-temperature dopant diffusion. All of these processes can be understood in terms of models and calculations based on macroscopic diffusion equations for heat and mass transport, cast in a finite-difference form to allow for the temperature and spatial dependences of the thermal conductivity, absorption coefficient, reflectivity, and other quantities. Results of calculations on silicon with the models show that the near-surface region of a sample can melt and stay molten for times of the order of 100 nsec during which dopant diffusion in the liquid state and nonequilibrium segregation during ultrarapid recrystallization are sufficient to explain the major features of the experimental results. In this paper, a description of the model used in our heat-transport calculations is given. Results of the modeling are illustrated by a variety of calculations which should be of particular interest to experimentalists working with pulsed-laser annealing. These results include, e.g., the effects of pulse duration, shape, and energy density, the effects of assumptions made about the latent heat of amorphous silicon, the effects of substrate heating, the role played by the absorption coefficient in determining melt-front penetration, and the duration of surface melting.

### I. INTRODUCTION

This is the first in a series of papers on the macroscopic theory of laser annealing by pulsed lasers. In these papers, we discuss the physical and mathematical models we have used during the past 2–3 years for calculations of heat transport and dopant diffusion during pulsed-laser annealing of ion-implanted silicon<sup>1–6</sup> and give selected results of the calculations. The same models have also been applied to laser-induced diffusion of surface-deposited dopants<sup>7</sup> and to recrystallization of doped amorphous silicon deposited on silicon substrates.<sup>8</sup> These three techniques for the laser-assisted doping of the near-surface regions of semiconductors have many features in common and for simplicity we will frequently use the term “laser annealing” to refer to them collectively. Most of the calculations of heat and mass transport are based on conventional macroscopic diffusion equations cast in a finite-difference formulation so that the space, time, and temperature dependence of various physical parameters such as the thermal diffusivity, specific heat, absorption coefficient of the laser radiation, etc., can be included in the models. A number of mechanisms for the interaction of the laser radiation with the sample will be listed but no attempt will be made here to assess the relative contributions of these mechanisms to the absorption coefficient. Also, the transfer of energy from the electronic system to the lattice will not be discussed except for

some fairly general observations. For these and other reasons we will refer to the development given in these papers as the macroscopic theory of pulsed-laser annealing, thus explicitly recognizing that extensive development of the microscopic theory is still required.

Our discussion will be restricted entirely to the melting model because the experimental evidence that melting occurs is very strong and because of the remarkable agreement between experiment and theory which is obtained with this model. The reflectivity change exhibited by semiconductors during intense laser irradiation has been studied since about 1964. In some of the earlier papers, this reflectivity change was attributed to the high density of photogenerated carriers, i.e., to an electron-hole plasma. However, Blinov *et al.*<sup>9</sup> concluded already in 1967 that this explanation did not fit their data on the absorption of long-wavelength radiation during irradiation of Si and GaAs with a high-power  $Q$ -switched ruby laser. They argued instead that the reflectivity change was due to the melting of a thin surface layer. A crucial question for the applicability of the melting model, at least in the form used here, concerns the lifetime of electron-hole pairs during intense laser irradiation and the transfer of energy from the electronic system to the lattice. There is a fairly substantial body of literature on this topic and virtually all of the experimental data indicate that the electron-hole recombination time is between  $10^{-11}$  and  $10^{-9}$  sec. In fact, Svantesson

*et al.*<sup>10</sup> found that in silicon the pulse width and shape of the recombination radiation in the region around 1.1 eV (indirect band gap of silicon) tracked the 30-nsec excitation pulse almost identically except for a very-low-intensity ( $\ll 1\%$  of primary) component which lasted for times of the order of a few microseconds. From the decay characteristics of the radiation, the authors concluded that the fast component of the recombination was due to Auger processes. In the earliest Soviet literature<sup>11</sup> on laser annealing it was recognized that melting of the near-surface region might explain a number of the experimental results on dopant profile spreading. However, the early results were not always consistent with one another and this led some Soviet investigators<sup>12</sup> to speculate that thermal models alone could not explain their results. These early experiments were carried out under conditions which were not ideal and the dopant profiling was done almost exclusively by the technique of anodic oxidation and stripping rather than by the more precise methods of Rutherford backscattering and SIMS (secondary ion mass spectroscopy). Furthermore, no detailed numerical calculations of temperature profiles, motion of the liquid-solid interface, and dopant redistribution were made. In fact, the calculations of Ref. 1 to interpret experimental data obtained at Oak Ridge National Laboratory (ORNL) and similar calculations by Baeri *et al.*<sup>13</sup> were the first to show convincingly that the near-surface region could melt and that dopant diffusion in the liquid state could explain the pronounced profile spreading which is observed after pulsed-laser annealing. At approximately the same time, experiments by Auston *et al.*<sup>14</sup> on the reflectivity change during laser annealing of Si and GaAs gave rather convincing evidence that surface melting did occur; other experiments subsequently reinforced this conclusion.<sup>15</sup> It is possible, in spite of the evidence to the contrary, to maintain that melting does not occur, that the reflectivity change is due to the very high density of laser-excited free carriers,<sup>16</sup> and that some form of "radiation-enhanced" diffusion is responsible for the long-range diffusion of dopants. A theory, which has yet to be constructed, along such lines would have in the end to give almost identical results to the theory discussed here and in the other papers of this series.

In this first paper, we concentrate on descriptions of the basic models for the heat-transport calculations, the computer program which has been used to implement the models, and some of the results of the calculations. The paper is organized into five sections. In the next section, the physical and mathematical models used in the

calculations are presented. In Sec. III, the computer code HEATING5<sup>17</sup> and its adaptation to laser annealing calculations are discussed. In Sec. IV, selected results of the calculations are given and these results and some of their implications are discussed in Sec. V. The last section contains some brief concluding remarks.

## II. PULSED-LASER ANNEALING

### A. Heat-diffusion equations

In the experimental situations assumed in this paper, the geometry of the sample and of the annealing configuration is such that ideally the heat-conduction problem is well represented by the one-dimensional diffusion equation.<sup>18</sup> The heat-generation function is determined by the interaction of the laser radiation with the sample and the subsequent transfer of the energy to the lattice. For a sample in which the materials parameters are dependent only on  $x$ , the differential equation for the temperature  $T(x, t)$  is

$$\frac{\partial T(x, t)}{\partial t} - \frac{\partial}{\partial x} \left( D \frac{\partial T(x, t)}{\partial x} \right) = P(x, t), \quad (1)$$

in which  $P(x, t)$  is the heat-generation function.  $D$  is the thermal diffusion coefficient which involves the thermal conductivity  $K$ , the specific heat  $c$ , and the density  $d$  of the sample material. The calculations will show that during pulsed-laser annealing, the temperature of the sample may be raised in a few nanoseconds from ambient to the melting point and even through the vaporization point, if the laser pulse is sufficiently energetic. Over these temperature ranges the thermal conductivity and specific heat are far from constant, as can be seen in Fig. 1. The thermal conductivity

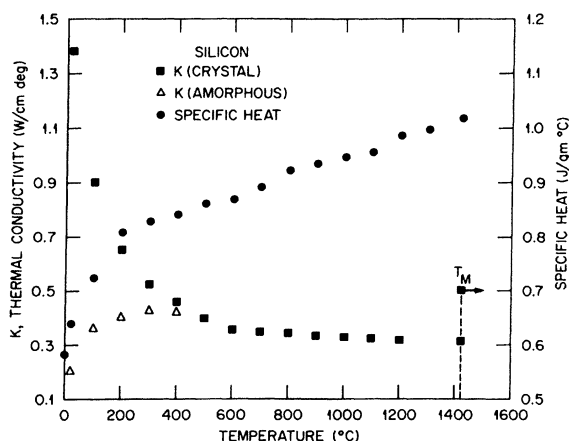


FIG. 1. Temperature dependence of the thermal conductivity and specific heat of silicon. The modification of  $K$  for the amorphous material is an estimate based on the behavior of glassy materials.

and specific heat data shown in Fig. 1 are from the compilation of Goldsmith *et al.*<sup>19</sup> More recent measurements<sup>20</sup> give somewhat different values which, however, have only small effects on a typical calculation. The value of  $K$  in molten silicon was found by relating the thermal to the electrical conductivity via the Wiedermann-Franz law.<sup>21</sup> Equation (1) cannot be used when  $D$  is strongly temperature dependent and phase changes occur, and a more complex formulation of the problem based on finite differences is required.

In finite difference form, Eq. (1) is replaced by a system of equations derived from a heat-balance condition at each of a set of points along the  $x$  axis. For the  $i$ th point not at a front or back surface this condition is expressed by

$$\frac{C_i(T_i^{n+1} - T_i^n)}{\Delta t} = P_i^n + \sum_{m=1}^{i+1} K_{i+m}(T_{i+m}^n - T_i^n). \quad (2)$$

$T_{i+m}^n$  is the temperature at time  $t_n$  of the  $i+m$  point immediately adjacent to the  $i$ th point,  $K_{i+m}$  is the thermal conductance between points  $i$  and  $i+m$ ,  $C_i$  is the heat capacitance of the material associated with point  $i$ , and  $P_i^n$  is the heat-generation rate in the latter material at time  $t_n$ . We have used a general-purpose heat-conduction computer program described in the next section to solve the system of equations.

#### B. Boundary conditions

In the few calculations carried out with Eq. (1), we assumed the boundary conditions

$$\left. \frac{\partial T(x, t)}{\partial x} \right|_{x=0} = 0 \quad \text{and} \quad T(x, t) \Big|_{x \rightarrow \infty} = \text{const}. \quad (3)$$

The first equation implies that no heat is lost from the front surface while the second reflects the fact that the sample is thick enough to act as a good heat sink. More complex boundary conditions were used in the finite-difference formulation. Both radiative and convective heat transfer from the front surface were allowed although the calculations almost invariably showed them to be negligible. For practical reasons, the finite-difference approach requires the sample to have a finite thickness and after some experimentation this thickness was chosen to be 10  $\mu\text{m}$ . The temperature of the back surface was assumed to be held at 20  $^\circ\text{C}$  except when otherwise noted.

#### C. Heat-generation function, reflectivity and absorption coefficient

In laser annealing, the reflectivity, effective absorption coefficient of the material, and energy-transfer rate to the lattice and the energy density and pulse duration time of the laser pulse largely

determine the heat-generation rate at each point in the sample. The function  $P_i^n$  in Eq. (2) can be written as

$$P_i^n = (1 - R_i^n)F_i^n \quad (4)$$

in which  $R_i^n$  is the reflectivity and  $F_i^n$  the absorption function for the  $i$ th layer at time  $t_n$ . Both  $R_i^n$  and  $F_i^n$  can be complicated functions of those material and physical parameters describing the  $i$ th layer at time  $t_n$ . A number of these parameters show large changes when the material undergoes a change of phase. Thus  $R_i^n$  and  $F_i^n$  can change continuously with time and distance as the melt front advances into the sample during the laser pulse. Although our computer program can handle such complexities, their inclusions would take large amounts of computer time and are difficult to justify at this stage in the development of laser annealing. The approximations we have made for treating the variations of  $R_i^n$  and  $F_i^n$  are discussed in the following paragraphs.

In all of our calculations thus far, we have assumed that reflection of the laser energy occurs entirely at the surface. Reflection of energy due to changing density, doping levels, lattice damage, etc., in layers beneath the surface layer are ignored except insofar as they contribute to an effective reflection coefficient at the surface. The reflectivity of silicon increases by about a factor of 2 when the material melts. This is the most important reflectivity effect in laser annealing and it is modeled in the calculations by providing a reflectivity switch which is activated when the material melts. Since reflection of light is not entirely a surface effect the question arises as to when the switch should be activated. After some experimentation we decided to let this occur when the melt front penetrated to a depth of 50  $\text{\AA}$ . Because of other uncertainties in laser annealing experiments and calculations this choice is not very crucial.

The reflectivity of amorphous silicon in the wavelength range of interest here is somewhat greater than that of perfect crystal silicon ( $\sim 0.40$  compared to  $\sim 0.32$ ) and high doping levels, lattice damage, surface roughness, thin films deposited on the surface, etc., may also alter the reflectivity. Because it would be virtually impossible to include all of these effects, we have generally allowed for only two different reflectivities which we denote by  $R_c$  and  $R_m$ , where  $c$  and  $m$  stand for crystalline (or solid) and molten, respectively. Only one measurement of the optical properties of molten silicon is reported in the literature before the laser annealing experiments of Ref. 14. From the data of Shvarev *et al.*,<sup>22</sup>  $R_m \approx 0.70$  at  $\lambda = 0.693 \mu\text{m}$  and normal incidence can be ex-

tracted; results in Ref. 14, however, suggest a somewhat smaller value. In virtually all of the calculations described in Refs. 3–8, a value of  $R_m = 0.60$  was used with satisfactory results. It is likely that uncertainties in the other input data are more than enough to compensate for small variations in the choice of  $R_m$ . Therefore for all of the calculations in this paper, with the exception of those leading to Fig. 2, we have taken  $R_c = 0.35$  and  $R_m = 0.60$ .

There are many discussions in the literature of the absorption mechanisms of intense laser radiation in solids. For our purposes the paper by Grinberg *et al.*<sup>23</sup> on the absorption of laser radiation and the creation of damage by that absorption gives a succinct summary. Those authors identify four absorption mechanisms likely to be important in semiconductors, i.e.,

- (1) Direct excitation of lattice vibrations by absorption of light with photon energy ( $h\nu$ ) well below the band-gap energy ( $E_g$ );
- (2) Excitation of free or nearly free carriers by absorption of light with  $h\nu < E_g$ ; such carriers will always be present as a result of finite temperatures and/or doping;
- (3) An induced metallic mechanism due to free carriers generated by the laser light itself;
- (4) Electron-hole excitation by light with  $h\nu > E_g$ .

In addition to these effects, which occur even in perfect crystals, the ion-implantation process itself alters the nature of the absorption in semiconductors. In undoped single-crystal Si, the absorption coefficient  $k$  at a wavelength of  $\lambda = 0.694 \mu\text{m}$  (ruby laser) and at low light intensities is approximately  $3 \times 10^3 \text{ cm}^{-1}$ .<sup>24</sup> Under the same conditions in amorphous Si,  $k$  increases to a value of  $\sim 5 \times 10^4 \text{ cm}^{-1}$ .<sup>25</sup> In ion-implanted semiconductors, the lattice damage created by implantation depends on the dopant, the implantation energy, and the dose. In many cases, such as 100-keV implantation of As in Si, the near-surface region is driven almost completely amorphous. We may expect that for most implantation conditions and wavelengths of laser radiation the energy will be absorbed in both the damaged and the undamaged regions of the sample. From these considerations, it can be seen that the absorption may vary strongly and in a complex manner with the distance from the front surface of the sample. Experimental data for the dependence of the absorption coefficient on position in the sample and on light intensity in circumstances approximating those encountered in laser annealing are still sparse. Thus, although the computer program we use can treat spatial- and intensity-dependent absorption, its full flexibility has not been used.

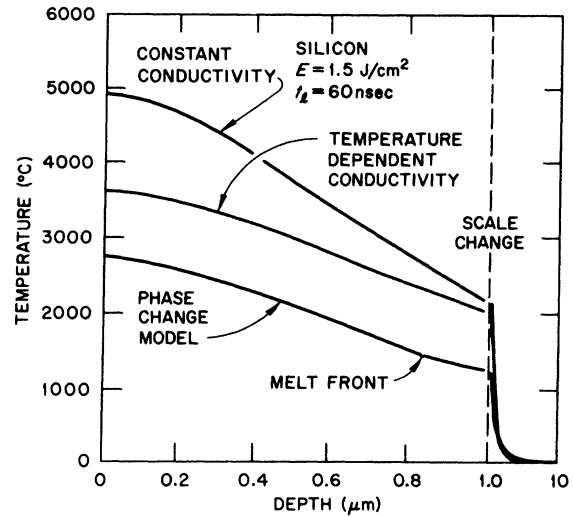


FIG. 2. Temperature profiles illustrating the effects of temperature-dependent thermal conductivity and specific heat and of melting.

The following approach has been used in the calculations. At low light levels, the change in light intensity  $dI$  due to absorption in a differential element of the sample is

$$dI = -k(x)I dx, \quad (5)$$

which integrates to

$$I(x) = I_0 \exp\left(-\int_0^x k(x_0) dx_0\right). \quad (6)$$

When  $k$  is independent of  $x_0$  this reduces to the usual simple exponential form. The form of  $I(x)$  which we have used most often in determining the  $F_i^n$  of Eq. (4) is obtained by assigning a constant value to  $k$  for those layers in the implanted, damaged, or noncrystalline region and another constant value for the layers in the crystalline or undamaged region. The sum of the  $F_i^n$  over the space and time intervals is, of course, normalized to give the total absorbed energy density. Calculations with more general assumptions about the spatial dependence of  $k$  have also been made on occasions but these calculations will not be discussed in this paper.

The absorption coefficient in silicon, like the reflectivity, is strongly dependent on the melting of the near-surface layer. In fact, molten silicon is metallic and thus  $k$  may increase from  $\sim 10^4 \text{ cm}^{-1}$  to  $\sim 10^6 \text{ cm}^{-1}$  when the near-surface region of the sample melts. In spite of this large change, the effects on the temperature calculations are not nearly as large as those produced by the change in reflectivity on melting. The reason for this will be discussed in Sec. V.

In this paper, we will consider that we have

three absorption coefficients to deal with, namely,  $k_c$  (crystalline region),  $k_d$  (doped or damaged region), and  $k_m$  (molten or metallic state).

#### D. Carrier diffusion

Recently, Yoffa<sup>26</sup> has carried out calculations which seem to imply that the diffusion of the hot, dense gas of electrons and holes generated during laser annealing plays a very important, if not dominant, role in determining the temperature rise of the lattice. The idea is that at the high excitation rates used in pulsed-laser annealing, the laser energy is given to the lattice within a characteristic depth determined primarily by carrier diffusion rather than by the absorption coefficient of the sample. The importance of carrier diffusion under conditions closely approximating those of laser annealing has been discussed previously by Blinov *et al.*,<sup>9</sup> who found the effect important in GaAs but not in Si. For reasons which we will discuss in Sec. V, we believe that our calculations show that carrier diffusion is a rather minor effect in most of the experiments we are attempting to model.

#### E. Latent heat of fusion

The latent heat of fusion is less for amorphous silicon than for single-crystal silicon and presumably the melting points differ also. Reliable information about these quantities in ion-implanted materials is not available. There are some indications that the latent heat of amorphous silicon may be roughly sixty percent of the single-crystal value and this has led to speculation that this would be an important effect in laser annealing. Our models have provisions for this difference in latent heat and we frequently make use of it. However, for reasons which we shall discuss later, the differences in latent heat are not likely to be of major importance in determining the melt-front position.

### III. DESCRIPTION OF THE COMPUTER PROGRAM HEATING5

#### A. Finite difference equation

The computer program HEATING5, is a general-purpose heat-conduction code previously developed at ORNL. It solves steady-state and transient heat conduction problems in one, two, and three dimensions for Cartesian, cylindrical, or spherical coordinates. The physical problem is approximated by a lattice of nodes, each associated with a small volume. Intersections of orthogonal planes define the nodal system. The planes may be unequally spaced, but of course they must extend

to the outer boundaries of the material system under consideration. Heat may flow between adjacent nodes along paths parallel to each coordinate axis. Thus, for a three-dimensional problem, flow occurs between an internal node and its six neighboring nodes. The system of equations describing the temperature distribution is derived from a heat-balance condition at each node. For example, the finite-difference, heat-balance equation for node  $i$  lying in the bulk of the sample is generalized from Eq. (2) to

$$\frac{C_i(T_i^{n+1} - T_i^n)}{\Delta t} = P_i^n + \sum_{m=1}^6 K_m^n (T_m^n - T_i^n). \quad (7)$$

Here,  $T_m^n$  is the temperature of node  $m$  adjacent to node  $i$  at time  $t_n$ ,  $K_m^n$  is the conductance between nodes  $i$  and  $m$ ,  $C_i$  is the heat capacitance of the material in the small volume around node  $i$ , and  $P_i^n$  is the heat-generation rate in this volume at time  $t_n$ . For a three-dimensional problem, one  $C$ , one  $P$ , and six  $K$ 's may be associated with each internal node at a particular time,  $t_n$ . By choosing the increments between nodal lattice points and time steps small enough, the solution to the system of equations yields an accurate approximation to the appropriate differential equation. Suitable space and time increments can be determined for each application by successive reduction in the increments until there is an acceptably small change in the solution. Space- and time-dependent heat generation and temperature-dependent thermal properties are relatively easy to incorporate into calculations with HEATING5. The time- and temperature-dependent properties can be given as tables and the program will interpolate to obtain the values required at any step.

#### B. Phase change

HEATING5 monitors the temperature at each node and therefore is able to recognize whether or not the material of a node is ready to undergo a phase change. If it is, the node's temperature is maintained at the transition temperature until the net heat content exceeds the node's latent heat of phase change. After the phase change, the node's temperature is again determined by the conductive heat-transfer equation. The ratio of the node's heat energy above that required to just reach the transition temperature to the latent heat required for phase change is called the transition ratio. The transition ratio can be interpreted either as a measure of the fraction of the node's material that has completed the phase change or as the extent to which *all* of the node's material has completed the phase change. In the former case, the node's volume is comprised of regions of solid

and liquid material separated by the phase interface. In the latter case, the node's volume contains material in a two-phase mixture sometimes referred to as "slush." In a heat-transfer problem dominated by conduction from a small region in which heat is generated, the former case will exist and the transition ratio can be used as an interpolating function to determine the location of the phase interface within the node's volume. This interpolating technique is easily applied to one-dimensional problems since the transition ratio is just equal to a fraction of the node's length. Its application to two- or three-dimensional problems is obviously not as straightforward.

When heat is generated nearly uniformly throughout extended regions of a sample (as with laser radiation of low absorption coefficients) it is possible for the material in those regions to undergo melting at approximately the same rate. A definite phase interface may be difficult to locate in such cases and the entire region can be a slush or transition zone. Transition zones have been observed in many of our calculations but with the conditions we emphasize here they disappear very quickly after the laser pulse has terminated.

#### C. Numerical methods (Ref. 27)

The point successive over-relaxation iterative method and a modification of the "Aitken  $\delta^2$  extrapolation process" are used in HEATING5 to solve the finite difference equations which approximate the partial differential equations for a steady-state problem. The transient problem may be solved using any one of several finite-difference schemes. These include an implicit technique which can range from Crank-Nicolson to the classical implicit procedure, an explicit method which is stable for a time step of any size, and the classical explicit procedure which involves the first forward time difference. The solution of the system of equations arising from the implicit technique is accomplished by point successive over-relaxation iteration, and includes procedures to estimate the optimum acceleration parameter. The time-step size for implicit transient calculations may be varied as a function of the maximum temperature change at a node. Transient problems involving materials with change-of-phase capabilities cannot be solved using the implicit technique with the present version of HEATING5. Therefore, the numerical method utilized in the heat-transfer analyses was the modified explicit technique or Levy method.<sup>5,17</sup> This technique allows stable calculations with time steps much larger than the node's stability criterion for the classical explicit method by utilizing a three-time-step explicit

scheme. (The stability criterion is the maximum allowable time step for a stable calculation with the classical explicit technique.) The Levy method enables a large reduction in computing cost for a transient analysis, with minimal loss of accuracy.

#### D. Space and time increments

Increments on the space and time grids can be chosen to give satisfactory results for a variety of closely related problems. Major extensions of a model to radically different conditions may require a redetermination of the space and time increments. These choices almost always involve a compromise between accuracy and computer time. In most of our calculations, we have used a minimum grid increment at the surface of  $1 \times 10^{-6}$  cm. This increment can be increased significantly in those regions of the crystal where the temperature is slowly varying. The time increment was allowed to vary with the laser power and/or pulse duration and ranged between  $2 \times 10^{-13}$  and  $10^{-11}$  sec.

### IV. CALCULATIONS AND RESULTS

#### A. Definition of two models and discussion of input data

Two basic models have been used in most of the calculations to be described below. In one model, the absorption coefficient is assumed to have some average, constant value throughout the sample; this is usually indicated on the figures by putting  $k_c = k_d$ . Such a model is suggested by (a) ion implantation of light ions such as boron in silicon where the implanted region is not made completely amorphous and the nature and extent of the damage is not very well defined, (b) multipulse annealing where it is known that after the first laser pulse the damage in the implanted layer may be completely removed, and (c) laser-induced melting of undoped, crystalline samples. Because of the absence of a well defined damaged region in these cases, we refer to this as the crystalline or *c* model. In the second model, a reasonably well defined amorphous region is assumed to be present. This model is expected to apply to the implantation of heavy ions into silicon in certain energy ranges and to samples on which an amorphous layer has been deposited by sputtering, *e*-beam deposition, etc. In the calculations, the absorption coefficient has one value ( $k_d$ ) in the damaged region and some other value ( $k_c$ ) in the undamaged, crystalline region. We will refer to this model as the amorphous or *a* model.

The input data for the calculations consists of the thermal conductivity *K*, specific heat *c*, density *d*, reflectivity *R*, absorption coefficient *k*, latent

heats of fusion (crystalline  $L_c$  and amorphous  $L_a$ ) and vaporization  $L_v$ , the corresponding temperatures  $T_c$ ,  $T_a$ , and  $T_v$  at which the phase changes occur, the starting temperature of the sample  $T_s$ , the laser-pulse shape, duration  $\tau_l$ , energy density  $E_l$ , and the parameters in the expressions for the radiative and convective heat transfer from the front surface. Most of these data are summarized in Table I and discussed below.

The density of silicon is only weakly temperature dependent in the solid but it increases by approximately 10% on normal melting of bulk samples. There is some indication that the lattice changes which occur during laser annealing of doped silicon are one-dimensional effects. This may imply that similar one-dimensional effects occur during the ultrarapid melting and resolidification characteristic of laser annealing and that the density change in the thin surface layer is significantly smaller than in bulk samples subjected to equilibrium melting. Because of uncertainties involved in other quantities we have kept the density fixed at  $d = 2.3 \text{ g/cm}^3$ . The specific-heat data given in Fig. 1 has been used in all of our calculations to date.

Limited calculations to test the sensitivity of the results to assumptions about  $K$ ,  $R$ ,  $L_a$ , and  $T_a$  have been carried out. Unless stated otherwise the data for  $K$  given by the solid squares in Fig. 1 has been used in the calculations. As al-

ready mentioned, in virtually all of the calculations discussed in this paper, the reflectivity of the solid material was taken to be 0.35 and that of the liquid 0.60. Later we may wish to distinguish more carefully between the reflectivity of the amorphous and crystalline material and also vary  $R_m$ , the reflectivity of the molten material. In those models where an amorphous layer is assumed to be present, we will generally take  $L_a = 0.6L_c$  and  $T_a = T_c$ . Further details of our choices of values for  $K$ ,  $R$ ,  $L_a$ , and  $T_a$  are given below. Extensive variations of the laser pulse parameters and of values of the absorption coefficient have been made and these will be discussed as we proceed.

#### B. Melting of near-surface region

Examples of the most important results of the temperature calculations are given in Figs. 2-5. Figure 2 shows calculated temperature profiles at the termination of a  $1.5 \text{ J/cm}^2$  ( $E_l = E$  on this figure), 60-nsec laser pulse. These results are from our earliest calculations with the  $c$  model in which the reflectivity was not allowed to change on melting; they are used here only for illustrative purposes. The top curve is a typical temperature distribution obtained from Eq. (1) when melting is not allowed and the thermal conductivity and specific heat are assumed to be constant with temperature. Comparison of the top and middle

TABLE I. Input data and symbols for the calculations.

Quantity	Symbol	Value and comments
thermal conductivity	$K$	see text and Fig. 1
specific heat	$c$	Fig. 1
density	$d$	2.3 (~10% change on melting ignored)
reflectivity		
solid	$R_s$	0.35 small differences between $R$ for crystalline and amorphous Si ignored
liquid	$R_m$	0.6 (see text)
absorption coefficient	$k_c, k_a$	see text
latent heats		
crystal	$L_c$	430 cal/g
amorphous	$L_a$	$0.06L_c$ (crude estimate)
vaporization	$L_v$	2535 cal/g
phase-change temperatures		
crystal	$T_c$	1410 °C
amorphous	$T_a$	1410 and 1000 °C (see text)
vaporization	$T_v$	2315 °C
substrate temperature	$T_s$	20 °C for most calculations
amorphous layer thickness	$X_a$	0.15 $\mu\text{m}$ for most calculations with the $\alpha$ model
laser pulse		
duration	$\tau_l, t_l$	varied
energy density	$E_l$	varied

curves shows the importance of the temperature dependence of  $K$  and  $c$ . The lowest curve was obtained from a calculation which allowed for a phase change (melting) as well as for temperature-dependent thermal conductivity and specific heat. This curve, indicates that the crystal melted to a maximum depth of almost  $0.85 \mu\text{m}$  at the termination of the laser pulse. However, because of the neglect of the reflectivity change on melting the

melt-front penetration is somewhat greater than it would be in a real sample.

Figures 3(a) and 3(b) show a series of temperature profiles at various times up to 200 nsec after 25-nsec pulses (FWHM) of  $E_i = 1.75 \text{ J/cm}^2$  and  $1.25 \text{ J/cm}^2$ , respectively. The crystalline model with  $k_c = k_d = 3 \times 10^4 \text{ cm}^{-1}$  and with a reflectivity increase from 0.35 to 0.60 on melting was used for these calculations. From data such as those

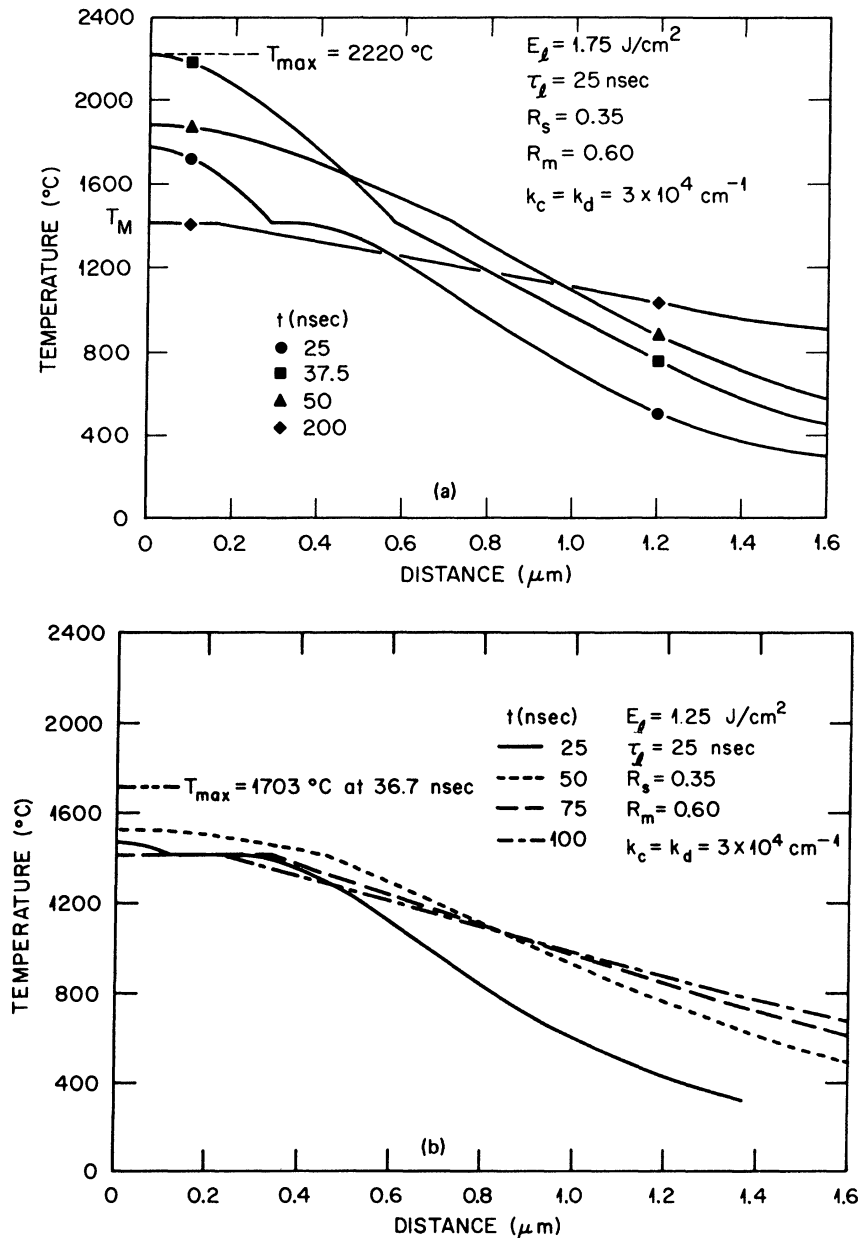


FIG. 3. (a) Temperature as a function of distance from the front surface of the sample at several different times during and after a 25-nsec,  $1.75\text{-J/cm}^2$  pulse. These results are for the  $c$  model in which the absorption coefficients  $k_d$  and  $k_c$  in the damaged and crystalline regions, respectively, have the same value. (b) The same as (a) but for a 25-nsec,  $1.25\text{-J/cm}^2$  pulse.

plotted on this figure and other data on the phase interface (Sec. IIIB), the position of the melt front as a function of time can be obtained. Illustrative results are shown in Fig. 4. In the calculation for a 1.5-J/cm<sup>2</sup> pulse, the melt front very rapidly penetrated to a depth of about 0.6  $\mu$ m in the solid, before receding back to the surface with the remarkably high velocity of  $\sim 4$  m/sec. While this occurred, a region about 0.3  $\mu$ m thick remained in the molten state for almost 100 nsec.

Figures 3 and 4 provide the key to understanding the physical basis of pulsed-laser annealing. Much of our work has been directed toward obtaining melt-front histories such as those contained in Fig. 4 for a variety of assumptions about the thermal conductivity, absorption coefficient, reflectivity, pulse duration time, etc. We turn now to examples of some of these calculations and to a number of questions of practical concern to experimentalists.

#### C. Effects of various assumptions about the thermal conductivity

The data for  $K$  (crystal) in Fig. 1 were used in virtually all of our calculations. There are many sets of thermal-conductivity data for Si in the literature and the discrepancies between the various sets are not always small. To test the sensitivity of our results to uncertainties in the values of  $K$ , we first carried out a calculation in

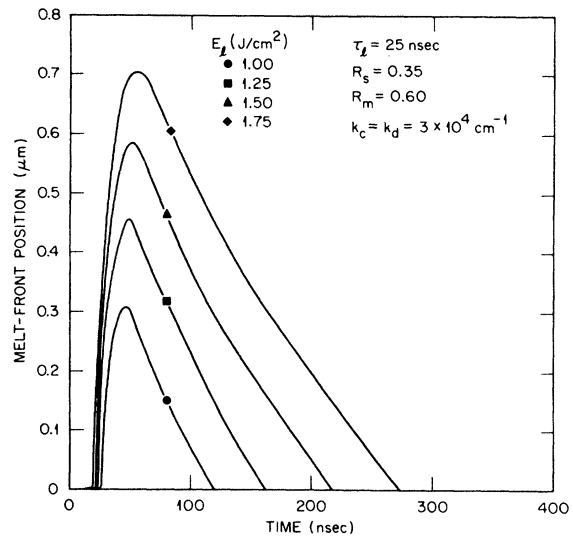


FIG. 4. Melt-front position as a function of time for the model used to obtain Fig. 3.

which  $K$  was arbitrarily decreased by 50% throughout the entire temperature range. In all other respects, the calculation was identical to that in Fig. 4 for the 1.25-J/cm<sup>2</sup> laser pulse. The results with and without the reduction are shown by curves marked with  $\blacktriangle$  and  $\blacksquare$ , respectively, on Fig. 5. The difference between the maximum melt-front penetrations for the two curves is not great but the differences between the melt-front velocities

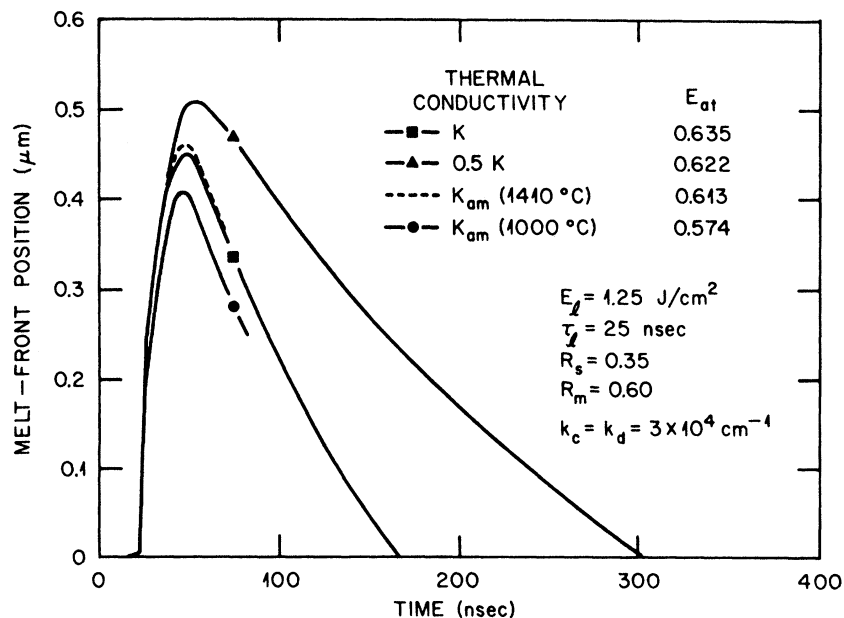


FIG. 5. Melt-front position as a function of time for calculations designed to test the effects of changing the thermal conductivity and melting temperature. On this figure, the subscript am stands for "amorphous";  $E_{at}$  is the total energy absorbed (J/cm<sup>2</sup>) during the laser pulse.

and the duration of surface melting are significant.

As already discussed in II C above, the ion-implantation process may make the implanted region almost totally amorphous. We do not know of any data in the literature on the thermal conductivity of amorphous silicon and its temperature dependence. However, from data on other amorphous and glassy materials,<sup>28</sup> we might expect  $K(T)$  to be modified in the low-temperature region to a form somewhat like that given by the open triangles on Fig. 1. With these modified data, denoted by  $K_{am}$ , we repeated the basic calculation of Sec. II C with the melting point held at 1410 °C and obtained the results shown by the dashed curve on Fig. 5. For the purposes of this test,  $K_{am}$  was assumed to hold for just the damaged region, which in 100-keV As-implanted silicon is only about 1500 Å thick; in the rest of the sample  $K(\text{crystal})$  was used. Of course, in the calculations of this section the thermal conductivity after melting and during resolidification was again assumed to have the crystalline values given by the solid squares in Fig. 1. It can be argued that the melting point of the amorphous material should also be made lower than that of the crystalline material. The curve marked with ● on Fig. 5 gives the results when the basic calculation is repeated with  $K_{am}$  and with the melting temperature lowered to 1000 °C. Again, the effects are not great. The reasons for this lack of sensitivity to the thermal properties of the amorphous region will be discussed in the next section.

#### D. Latent heat in the amorphous layer

In this subsection, we consider the effects of reducing the latent heat of fusion in the amorphous layer, i.e., of taking  $L_a < L_c$ . The results of these calculations are shown in Fig. 6. In the calculations, we assumed  $X_a = 0.15 \mu\text{m}$ ,  $k_a = 5 \times 10^4 \text{ cm}^{-1}$ ,  $k_c = 3 \times 10^3 \text{ cm}^{-1}$ ,  $R_s = 0.35$ , and  $R_m = 0.60$ . Curve *a* gives the melt-front history for a laser pulse of  $E_i = 1.4 \text{ J/cm}^2$ ,  $\tau_i = 15 \text{ nsec}$ , and with  $L_a = L_c$  and curve *b* is for the same laser conditions but with  $L_a = 0.6L_c$ ; in both cases the melting temperature of the amorphous and crystalline regions was 1410 °C. Curves *c* and *d* are for the same sequence of calculations but with  $E_i = 1.5 \text{ J/cm}^2$  and  $\tau_i = 60 \text{ nsec}$ . Clearly, a substantial reduction in the latent heat does not cause large changes in the melt-front histories for the sample and laser annealing conditions used here. For samples with thicker amorphous layers, the melt-front penetration may be somewhat more strongly affected by the latent heat difference. This will be discussed further in Sec. V.

#### E. Effects of pulse shape, duration, and energy density

During the operation of a Q-switched laser for laser annealing the energy density may be varied over wide ranges deliberately to control the depth of melting. However, there will also be fluctuations from pulse to pulse in the energy density, the pulse duration time, and the pulse shape, and the experimentalist needs to know how critical these fluctuations are to the annealing process. We consider these questions next.

**Pulse shape.** Figure 7 shows melt-front histories for a number of different pulses of radically different shape for which the total energy incident on the sample is the same. The symbols for pulse shapes on the figure should be self-explanatory, with the possible exception of the dashed curve which is for a Gaussian. It is clear from these results that large variations in the pulse shape can alter the melt-front penetration. However, pulse shapes which are reasonably close to Gaussian will give quite similar melt-front histories. In fact, we used an isosceles triangle for the pulse shape in the rest of the calculations described in this paper because it is somewhat easier to handle numerically and gives essentially the same results as a Gaussian.

**Pulse duration.** The results of calculations to test the sensitivity of melt-front penetration to the pulse-duration time (full width at half maximum) are given in Fig. 8. The figure shows that the melt-front history is fairly sensitive to variations in the pulse duration. Nonetheless, it would seem that pulses of a well tuned laser can be controlled to the degree that is needed in most laser

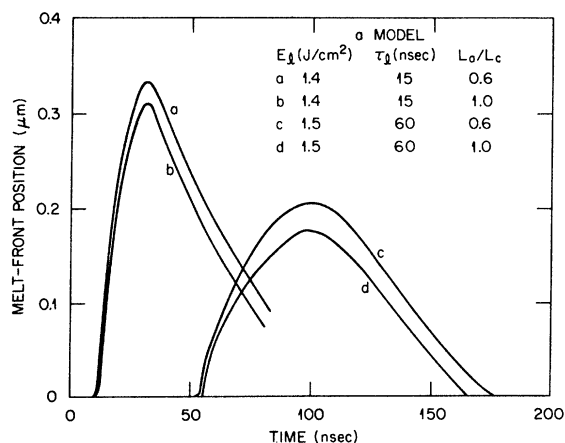


FIG. 6. Effects on the melt-front profile of a 40% reduction in the latent heat of phase change. The *a* model with an amorphous layer 0.15  $\mu\text{m}$  thick was used for these calculations;  $R_s = 0.35$ ,  $R_m = 0.60$ ,  $k_a = 5 \times 10^4 \text{ cm}^{-1}$ , and  $k_c = 3 \times 10^3 \text{ cm}^{-1}$ .

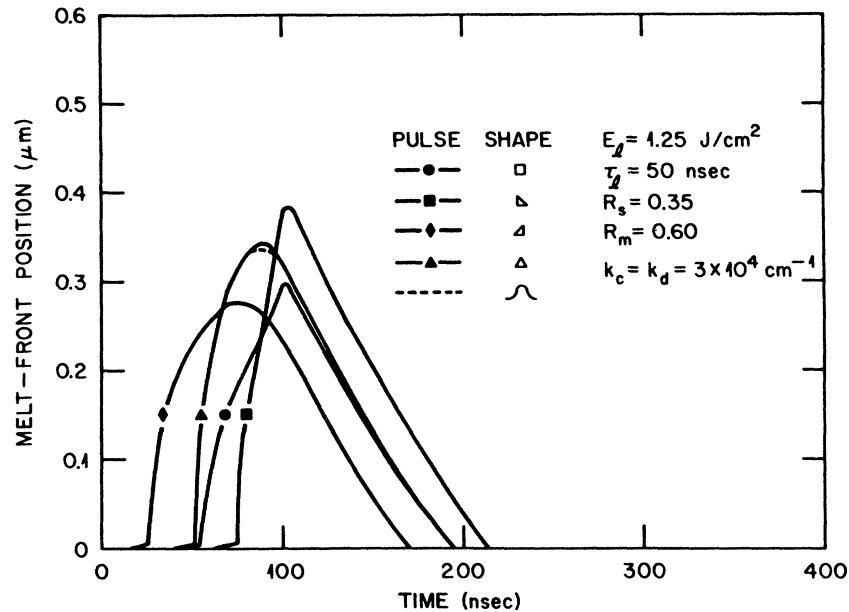


FIG. 7. Effects of pulse shape on melt-front profiles. The dashed curve is for a Gaussian pulse shape. All pulses contained exactly the same energy.

annealing experiments without too much difficulty. For example, the differences between melt-front histories for a 15-nsec and a 20-nsec pulse are not likely to be important when the other experimental uncertainties are considered. However, these calculations show that laser pulses of the same energy density but widely different duration will produce quite different melt-front profiles.

The dashed line on the 200-nsec curve shows the slush or transition zone discussed in Sec. II. All of the curves on the figure have slush zones associated with them but, to avoid confusion, they have not been shown. For short pulses they do not penetrate deeper than the fully melted zone and they exist for only very brief periods. The hook on the short-time edge of each curve is both

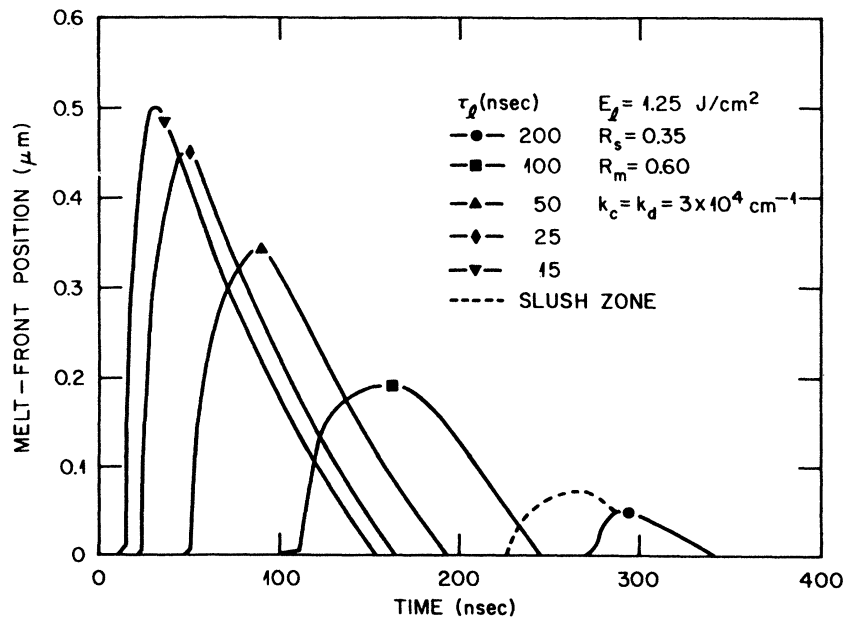


FIG. 8. Effects of pulse duration (FWHM) on melt-front profiles for a 1.25-J/cm<sup>2</sup> pulse. The *c* model ( $k_c = k_d$ ) was used for these calculations. The "slush zone" is explained in the text.

a manifestation of the slush zone and an approximate indication of how long it lasts. By increasing the pulse duration beyond 200 nsec the duration of the slush zone can be increased for this 1.25-J/cm<sup>2</sup> pulse, but eventually of course a duration will be reached for which the melting temperature is never attained.

We have carried out several calculations for ultrashort pulses using the *a* model with  $X_a = 0.15$   $\mu\text{m}$ ,  $k_d = 5 \times 10^4$  cm<sup>-1</sup>, and  $k_c = 3 \times 10^3$  cm<sup>-1</sup>. These calculations show that the trends in Fig. 8 continue as the pulse duration time decreases. They will be discussed in more detail in Sec. V in connection with the control of melt-front velocity.

*Pulse energy density.* By plotting data such as those contained in Fig. 4 in a different way, the variation of the maximum melt-front penetration with either the incident or absorbed energies can be displayed. Figure 9 shows how the melt-front penetration varies with *absorbed* energy for both the amorphous and the crystalline models. The calculations using the *a* model were carried out for three different values of the absorption coefficient in the damaged region, i.e.,  $k_d = 5, 6,$  and  $8 \times 10^4$  cm<sup>-1</sup>; outside of the damaged region, we took  $k_c = 3 \times 10^3$  cm<sup>-1</sup> as in the other calculations. The amorphous layer was 0.15  $\mu\text{m}$  thick. For the *c* model,  $k_d = k_c = 3 \times 10^4$  cm<sup>-1</sup> as in Fig. 4. The

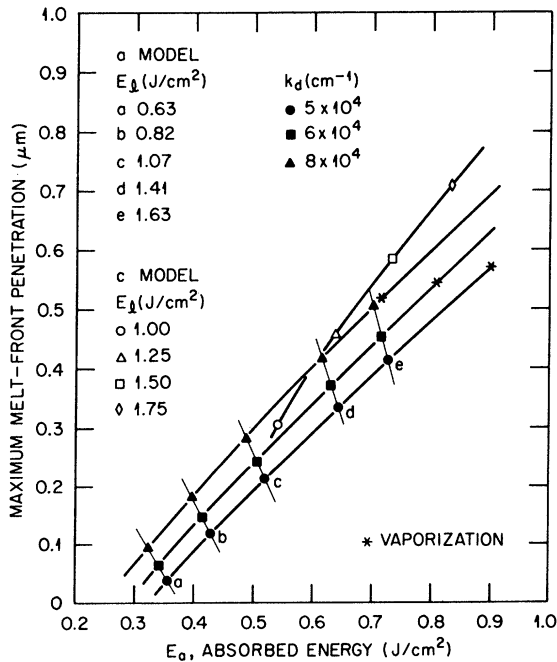


FIG. 9. Maximum melt-front penetration as a function of absorbed energy for the *a* and *c* models. In the *a* model, the amorphous or damaged layer was 0.15  $\mu\text{m}$  thick. The asterisk indicates the onset of vaporization at the surface.

data in the figure legend give the incident energy for each of the points indicated. By comparing the incident energy to the absorbed energy one can see that the latter is generally speaking roughly half of the former for both models. This is primarily a reflectivity effect and shows, not unexpectedly, that techniques for reducing reflectivity losses could result in a substantial reduction of the energy density needed for laser annealing. The figure also shows that the melt-front penetration is fairly strongly dependent on the value assumed for  $k_d$  in the *a* model. The primary reason for this effect is simply that as  $k_d$  is increased the percentage of the laser energy absorbed in the amorphous layer increases rapidly and the heat is used more effectively for melting the near-surface region. Obviously, the thickness of the amorphous layer also plays an important role in determining the melt-front penetration as we shall see next. It should be noted from Fig. 9 that the material at the surface vaporizes at increasingly lower energies as  $k_d$  is increased.

#### F. Thickness of the amorphous layer

Although an amorphous layer thickness  $X_a$  of 0.15  $\mu\text{m}$  has been assumed in most of our calculations with the *a* model, the effects of varying  $X_a$  have also been tested. Some of the results are shown in Table II for both  $L_a = 0.6L_c$  and  $L_a = L_c$ . It can be seen from this table that the differences in penetration depth between the two cases increases somewhat as  $X_a$  increases. This occurs because the percentage of the pulse energy which is required to supply the latent heat of melting of the amorphous layer increases with  $X_a$  faster for  $L_a = L_c$  than it does for  $L_a = 0.6L_c$ .

#### G. Effects of varying the absorption coefficient

For reasons briefly discussed in Sec. II C, the absorption of radiant energy by a semiconductor and its deposition in the lattice is a complex phe-

TABLE II. Maximum penetration of the melt front for various thicknesses of the amorphous layer and for two different assumptions about the latent heat of the amorphous layer. Values of the main parameters for the calculation were  $E_i = 1.5$  J/cm<sup>2</sup>,  $\tau_i = 15$  nsec,  $k_d = 5 \times 10^4$  cm<sup>-1</sup>,  $k_c = 3 \times 10^3$  cm<sup>-1</sup>,  $R_s = 0.35$ , and  $R_m = 0.60$ .

$X_a$ ( $\mu\text{m}$ )	Melt-front penetration	
	$L_a/L_c = 0.6$	$L_a/L_c = 1.0$
0.10	0.285	0.248
0.15	0.382	0.344
0.20	0.452	0.406
0.25	0.524	0.451
0.30	0.587	0.494

nomenon. Describing this process by one ( $c$  model) or two ( $a$  model) simple exponential forms as we have done in our calculations are approximations which will need further study as the macroscopic theory of laser annealing is developed. Here we show the effects of varying the absorption coefficient in the  $c$  and  $a$  models.

Three curves of melt-front penetration as a function of  $k_c$  in the  $c$  model are given in Fig. 10. Two features of these curves are of particular interest. First, we note that the penetration depths appear to rapidly approach limiting values as  $k_c$  is increased. If vaporization did not occur (it does not for the data we show), the asymptotic limit would presumably be reached as  $k_c \rightarrow \infty$ , i.e., when all the energy is deposited in a very thin surface layer. The fact that the curves for the  $c$  model have this behavior has a practical consequence. When the near-surface region of the sample melts, not only does the reflectivity increase by nearly a factor of 2, the absorption coefficient should increase to metallic values ( $\sim 10^6 \text{ cm}^{-1}$ ). The HEATING5 program, and presumably most finite-difference calculations, requires long running times to obtain accurate solutions to problems in which the absorption coefficient is as high as  $10^6 \text{ cm}^{-1}$ . Figure 10 shows that with the  $c$  model when  $k_c \geq 2 \times 10^4 \text{ cm}^{-1}$ , results which are accurate enough for most purposes can be obtained without switching  $k_c$  to a high value when the surface melts. We have carried out calculations with  $k_c$  switched to  $10^6 \text{ cm}^{-1}$  on melting which confirm this. The second feature of the  $c$ -model results which interests us is the behavior of the curves at low values of  $k_c$ . As  $k_c$  is decreased, the laser energy is deposited more uniformly throughout the sample and eventually, for a given  $E_l$  and  $\tau_l$ , a value of  $k_c$  is reached for which enough heat to cause melting cannot be

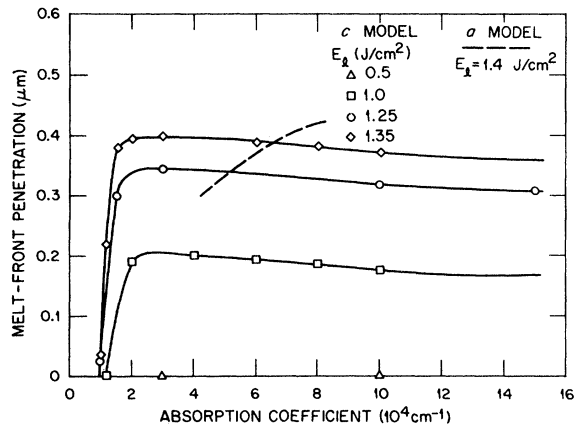


FIG. 10. Data on the maximum melt-front penetration as a function of absorption coefficient.

supplied to any volume element of the sample. It is in the calculations with small values of  $k_c$  and/or long pulse times, that the transition or slush zones discussed in Sec. IIB become most noticeable. The slight decrease in the penetration with increasing absorption coefficient is due to the reflectivity change at melting. Calculations with a constant reflectivity have constant penetrations as  $k_c$  increases.

The situation is more complex for the  $a$  model, as can be seen from the dashed curve on Fig. 10. For a given thickness of the amorphous layer and with the laser-pulse parameters fixed, increasing the value of the absorption coefficient will cause more and more of the laser energy to be deposited in the amorphous layer and thus the melt-front penetration will increase more rapidly than it does in the  $c$  model. When the absorption coefficient  $k_a$  is great enough that essentially all of the energy is absorbed in the damaged layer, further increases in  $k_a$  should produce the asymptotic behavior characteristic of the  $c$  model.

The reader should recognize that temperature effects, free carrier absorption by carriers excited by the light itself, and possibly other effects will be particularly important when the absorption coefficient due to direct excitation of electron-hole pairs is low. For these and other reasons, e.g., carrier diffusion, the distinction between the crystalline and amorphous models is not as clear cut in reality as we have made it in our calculations.

#### H. Substrate heating

As the next example of the temperature calculations, we show in Figs. 11 and 12 results for a series of cases in which the sample was either cooled or heated while the laser annealing was carried out. Substrate heating is of interest for several reasons. If, for example, an available laser cannot supply the energy required to melt

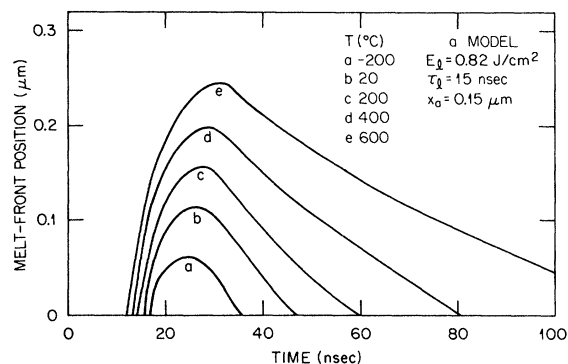


FIG. 11. Effects of substrate heating on melt-front profiles for a 15-nsec, 0.82-J/cm<sup>2</sup> pulse.

the near-surface region to a particular depth, sample heating may extend the melting range to that depth. The calculations of Fig. 11 were carried out for samples irradiated with single pulses of  $0.82 \text{ J/cm}^2$  and 15-nsec duration. The results show that the melt-front penetration depth can be extended by almost a factor of 2 by increasing the sample temperature from  $20^\circ\text{C}$  to about  $500^\circ\text{C}$ . Even if a laser has sufficient power it may still be advantageous to use substrate heating so that the lowest possible energy density for annealing can be used. In this way, the magnitude of the spatial inhomogeneities in the laser energy can be reduced. Probably the most interesting use of substrate heating and cooling at this time would be to control the melt-front velocity during resolidification of the melted near-surface region. Control of the melt-front velocity will be discussed in the next section.

#### I. Duration of surface melting

Thus far we have not discussed the agreement between our calculated results and the available experimental data. Such a discussion will rely primarily on comparisons between calculated and experimental dopant profiles and we will not consider these until the next paper in this series. However, results reported by Auston and co-workers<sup>14,29</sup> on the duration of surface melting as a function of laser-pulse energy density do not involve dopant diffusion and can be considered here.

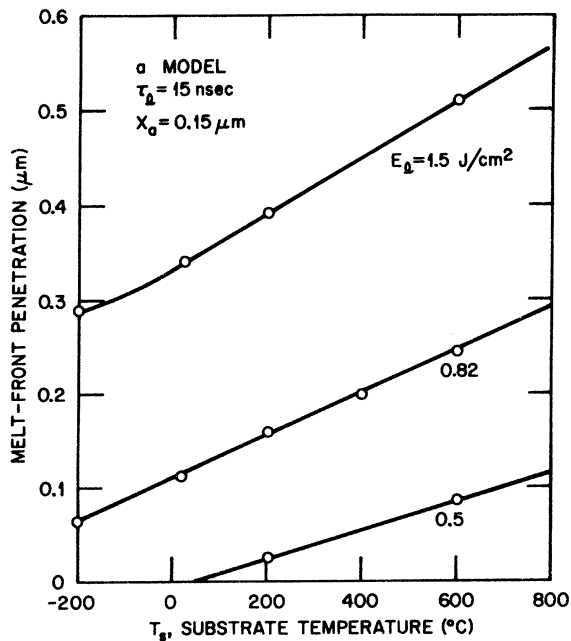


FIG. 12. Maximum melt-front penetration as a function of substrate temperature in the *a* model.

In their first paper on the subject, Auston *et al.*<sup>14</sup> studied surface melting of As-implanted Si during laser annealing with a Nd:YAG laser operating in the fundamental ( $\lambda = 1.06 \mu\text{m}$ ). In more recent papers,<sup>23</sup> the melting of both pure and implanted Si and GaAs samples irradiated with the fundamental and frequency-doubled radiation of a Nd:YAG laser was studied. Experimental data for 30-keV As-implanted Si are shown by the solid circles on Fig. 13. The points designated as "c model" (■) were obtained from early calculations in which  $\tau_i = 50 \text{ nsec}$ ,  $k_c = k_d = 3 \times 10^4$ ,  $R_s = 0.35$ , and  $R_m = 0.60$ . We subsequently carried out calculations with a set of parameters ( $\tau_i = 33 \text{ nsec}$ ,  $k_d = k_c = 10^5 \text{ cm}^{-1}$ ,  $R_s = 0.35$ ,  $R_m = 0.60$ ) used by the Bell Laboratories authors (Ref. 29) in their calculations on undoped silicon; the results are shown by the  $\blacktriangle$  points on Fig. 13. Within the limits set by experimental error and uncertainties in the input data for the calculations, the results of the experiments and the two sets of calculations are indistinguishable except, perhaps, at very low incident energies where there appears to be an inflection in the experimental data not given by the calculations. We cannot say if this is a real effect at this time.

The open circles and squares are calculated data obtained from the *a* model with an amorphous layer  $X_a = 0.15 \mu\text{m}$  thick and an absorption coefficient in this region of  $k_d = k_a = 8 \times 10^4 \text{ cm}^{-1}$  and  $5 \times 10^4 \text{ cm}^{-1}$ , as indicated on the figure; for the

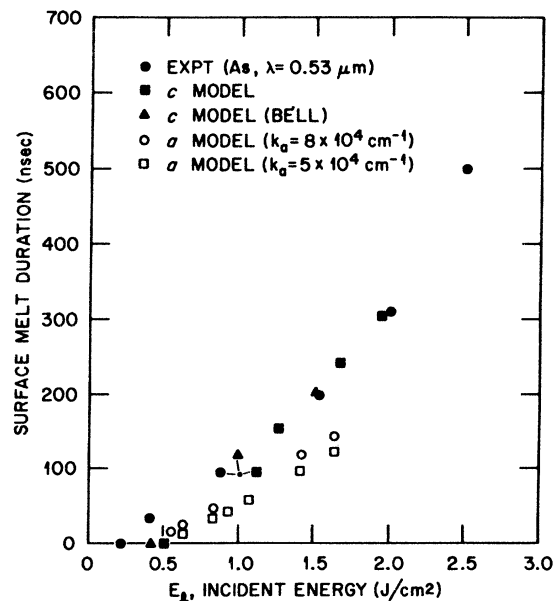


FIG. 13. Data on the duration of surface melting as a function of incident laser energy. On this figure, the absorption coefficient in the  $0.15\text{-}\mu\text{m}$  amorphous layer is indicated by  $k_a$  rather than  $k_d$ .

region deeper than  $X_a$  we again took  $k_c = 3 \times 10^3 \text{ cm}^{-1}$ . The differences between the surface-melt duration times for a given incident energy calculated with the  $a$  and  $c$  models are large. We carried out a series of calculations to establish the principal source of these differences. These calculations were based on the recognition that our choice of  $k_c = 3 \times 10^3 \text{ cm}^{-1}$  in the undamaged region in the  $a$  model is somewhat arbitrary and probably unrealistic. This choice would be appropriate to the absorption of  $0.693\text{-}\mu\text{m}$  radiation by undoped single-crystal silicon at room temperature and low-light intensity, but it is unlikely that it applies under the conditions of laser annealing. Figure 10 shows that this value of  $k_c$  used in the  $c$  model does not produce any melting of the sample even for  $E_i = 1.35 \text{ J/cm}^2$ . The experiments in Ref. 29 show that the surface-melt duration at a given incident energy density for undamaged and undoped Si and for the 30-keV As-implanted samples (see Fig. 13) differ very little. In order to fit these data we assumed a value of  $k_c = 3 \times 10^4 \text{ cm}^{-1}$  in our  $c$ -model calculations and the Bell group assumed  $k_c = 10^5 \text{ cm}^{-1}$  in similar calculations. From this it seems quite evident that temperature effects and induced free carrier absorption [mechanisms (2) and (3) of Sec. II C] are playing an important role in determining  $k_c$ . In the  $a$  model, the importance of the value chosen for  $k_c$  will depend on the value of  $k_d$  used in the amorphous layer and on  $X_a$ , the thickness of the layer. When the laser radiation is entirely absorbed in  $X_a$ , the value of  $k_c$  is irrelevant. A series of transient reflectivity experiments on samples with a range of values of  $X_a$  would be very useful as an aid in the "calibration" of the calculations.

## V. DISCUSSION

In this section, the results in the preceding section and other results of the computer calculations will be used as a basis for discussion of several features of pulsed-laser annealing that are of current interest.

### A. Thermal gradients at the liquid-solid interface

Most theories of crystal growth<sup>30</sup> relate the crystallization rate to the temperature of the liquid-solid interface. In practice, this temperature is not well defined and virtually impossible to measure at the melt-front velocities involved in laser annealing. Moreover, in terms of the macroscopic diffusion equations used here, it is the temperature *gradients* at the melt front which are important in determining the melt-front velocity. From Figs. 3(a) and 3(b) it can be seen

that the liquid-solid interface is always at the melting temperature [indicated by  $T_M$  on Fig. 3(a)]; in fact, this is one of the boundary conditions of the problem. Another boundary condition is the equation (recall that  $d$  is the density)

$$Lvd = K_m G_{mi} - K_s G_{si}. \quad (8)$$

For simplicity of notation, the temperature gradients at the interface in the liquid and solid are written as  $G_{mi}$  and  $G_{si}$ , respectively;  $K_m$  and  $K_s$  are the corresponding thermal conductivities, and  $v$  is the melt-front velocity. The latent heat  $L$  during recrystallization is  $L_c$  of Table I. Table III shows these gradients for the curves on Figs. 3(a) and 3(b); the gradients are very large and explain the high melt-front velocities observed in laser annealing.

It should be noted from Fig. 3(a) that for a  $1.75\text{-J/cm}^2$  pulse, the surface reaches  $2220^\circ\text{C}$  which is only  $100^\circ\text{C}$  lower than the vaporization temperature. In such cases, large temperature gradients may exist in the liquid for extended periods of time and this could influence the diffusion of dopants in the liquid. The maximum temperature for the  $1.25\text{-J/cm}^2$  pulse is  $1703^\circ\text{C}$  which is only  $300^\circ\text{C}$  above the melting point of silicon. Most laser annealing of silicon for device applications is likely to be done at  $1.1\text{--}1.4 \text{ J/cm}^2$  and the temperature of the molten zone is not expected to rise much above  $T_M$  for any appreciable time. Thus, we would expect dopant diffusion in the liquid to be characteristic of diffusion near the melting point.

In these calculations, which do not include the effects of dopants on the thermal properties, such as the melting point of the material, consideration of constitutional supercooling is automatically excluded and ordinary supercooling apparently does not occur. Thus, in Figs. 3(a) and 3(b) the temperature of the liquid never falls below  $T_M$  for silicon. Cellular structure in the distribution of some dopants in Si after laser melting has been observed<sup>31,32</sup> and this is a clear indication that significant constitutional supercooling does occur under some conditions. It would be difficult to

TABLE III. Temperature gradients in units of  $^\circ\text{C/cm}$  at the melt front for the curves in Figs. 3(a) and 3(b).

$t$ (nsec)	$E_i = 1.75 \text{ J/cm}^2$		$E_i = 1.25 \text{ J/cm}^2$	
	$G_{mi}$	$G_{si}$	$G_{mi}$	$G_{si}$
25	$1.79 \times 10^7$	$1.01 \times 10^6$	$0.96 \times 10^7$	$1.33 \times 10^7$
37.5	$2.04 \times 10^7$	$0.95 \times 10^7$		
50.0	$9.63 \times 10^6$	$1.25 \times 10^7$	$5.17 \times 10^6$	$9.0 \times 10^6$
75.0			$1.33 \times 10^4$	$6.57 \times 10^6$
100.0	$7.33 \times 10^4$	$0.57 \times 10^6$	$<1.3 \times 10^4$	$5.5 \times 10^6$
200.0	$<10^4$	$0.37 \times 10^6$		

take the effects of the dopants on the thermal properties of silicon into account directly in the temperature calculations but it may be possible to add them later in a perturbation approach.<sup>33</sup>

#### B. Control of melt-front velocity

Values of the equilibrium interface segregation coefficient  $k_i^0$  for B, P, and As in Si (Ref. 34) are 0.80, 0.35, and 0.3, respectively. Standard theories of crystallization under equilibrium conditions,<sup>35</sup> applied to the laser-annealing process, show that in As- and P-implanted Si these values of  $k_i^0$  should produce concentration spikes at the surface; these surface spikes are not observed<sup>36, 8</sup> and satisfactory fits to the dopant profiles in these cases can only be obtained with values of  $k_i$  nearly equal to unity.<sup>1, 8</sup> Recently White *et al.*<sup>37</sup> used Rutherford backscattering (RBS) techniques to measure the profiles of As, Sb, Ga, In, and Bi in ion-implanted, laser-annealed Si. From fits of the measured profiles, values of  $k_i$  were extracted. The results in Refs. 1, 8, 36, and 37 provide data on the segregation behavior of B, P, As, Sb, Ga, In, and Bi in Si during laser annealing. The most striking feature of these results is the very large differences between  $k_i^0$  and  $k_i$ , particularly when  $k_i^0$  is small. The increase of  $k_i$  over  $k_i^0$  is almost certainly a nonequilibrium effect due to the large recrystallization velocities encountered in laser annealing.<sup>38</sup> Hence, control of the melt-front velocity  $v$  becomes particularly important in the testing of various models of nonequilibrium segregation during ultrarapid recrystallization.

The results of the calculations of the preceding section, suggest several methods for controlling  $v$ . These include substrate heating, alteration of the thermal conductivity of the base region, and variation of the pulse duration time. Substrate heating is undoubtedly the most easily accessible experimental technique for control of the melt front and we will discuss it first.

Values of  $v$  can be found from any of the curves of melt-front position as a function of time by taking the derivative with respect to time. The recrystallization velocity is clearly not constant, but an average velocity is sufficient at the present stage of the development of laser annealing. Estimates of  $v$  from Fig. 11 show that variations of factors of 2–3 in the average values during recrystallization can be produced by substrate heating in easily accessible temperature ranges. Variations of this magnitude should be sufficient to allow limited studies of the effects of  $v$  on dopant segregation during laser annealing.

The curves on Fig. 5 suggest that an effective

method for controlling the melt-front velocity would be to modify the thermal conductivity of the substrate region. This could be done by depositing thin ( $< 1 \mu\text{m}$ ) films of silicon on substrates with very low thermal conductivity. Melt-front calculations on a sample consisting of  $0.5 \mu\text{m}$  film of Si on an  $\text{SiO}_2$  substrate showed that the melt-front velocity could be reduced to 1.5 m/sec. A possible difficulty with this method is that the Si film will not normally be expected to recrystallize as single-crystal Si and this could alter the segregation effects somewhat.

A third method for controlling  $v$  is suggested by the data on Fig. 8 which indicate that there is at least a weak dependence of the melt-front velocity on pulse duration time. We carried out calculations with the amorphous model ( $X_a = 0.15 \mu\text{m}$ ,  $k_a = 5 \times 10^4 \text{ cm}^{-1}$ ,  $k_c = 3 \times 10^3 \text{ cm}^{-1}$ ) for pulses of  $E_i$  and  $\tau_i$  combinations of (0.85 J/cm<sup>2</sup>, 16 nsec), (0.82 J/cm<sup>2</sup>, 1.6 nsec), (0.41 J/cm<sup>2</sup>, 1.6 nsec), and (0.41 J/cm<sup>2</sup>, 0.16 nsec). The results showed that  $v$  increased by about a factor of 2 in going from the 16-nsec to the 1.6-nsec pulse. The 0.16-nsec pulse resulted in a slight further increase in the velocity but at these short pulses, vaporization of the surface becomes an important factor. The results of these calculations were consistent with the data of Fig. 8 insofar as the maximum melt-front penetration is concerned. For example, the penetration for the 1.6-nsec pulse was almost twice as great as that for the 16-nsec pulse, which is roughly comparable to the percentage increases in going from a 100- to a 15-nsec pulse. Also, the 0.41-J/cm<sup>2</sup>, 0.16-nsec pulse achieved almost the same penetration as the 0.82-J/cm<sup>2</sup>, 1.6-nsec pulse even though vaporization limited the penetration achieved with the former pulse.

It should be noted that attempts to modify the melt-front velocity will also produce variations in the melt-front penetration and this in turn will effect the dopant redistribution. Because of this, it appears that meaningful results of experiments designed to test the effects of melt-front velocity on the segregation of dopants during laser annealing can only be obtained after fairly extensive calculations and theoretical fits to the experimental data.

#### C. Effects of thermal properties of the amorphous region

Figures 5 and 6 are concerned with the influence of the thermal properties of the amorphous material on the melt-front profiles. We have seen that these effects are relatively small in the range of annealing conditions used here and we now explore the reasons for this somewhat surprising

result. Table IV gives some data pertinent to this question provided by the computer calculations. In this table,  $t_{m1}$  is the time after the initiation of the laser pulse at which the average temperature of a surface layer 50 Å thick reaches melting temperature and  $t_{m2}$  is the time at which the surface cell absorbs enough latent heat to complete the phase transition;  $E_{m1}$  and  $E_{m2}$  are the corresponding absorbed energies.  $E_{at}$  is the total energy absorbed by the sample throughout the laser pulse,  $d_{max}$  is the maximum penetration of the melt front, and  $T_{max}$  is the maximum temperature the surface reached. The first two lines of the table show that a 50% reduction in the thermal conductivity results in a very small decrease in  $E_{at}$ . However, because of the reduced thermal conductivity, the energy is more effective in raising the temperature of the surface and in melting the near-surface region. Comparison of lines 1 and 3 of Table IV show that the assumed modification of  $K$  for amorphous silicon shown in Fig. 1 has very little effect on the melt-front behavior. Apparently, this is because the modification of  $K$  is only in the low-temperature regime through which the temperature of the sample passes very quickly. Comparison of line 4 with lines 1–3 of Table IV shows that the lower-melting temperature (1000 °C) of line 4 results in the sample melting sooner and with less absorbed energy ( $E_{m2}$ ) than is the case with the 1410 °C melting temperature (lines 1–3). However, because the reflectivity switch cuts in sooner for the lower-melting-temperature material, the total absorbed energy is actually less than for the other cases.

The effects of a reduction in the latent heat by 40%, as given in rows 5–8 of Table IV, are also not large for an amorphous layer 0.15 μm thick. There is some evidence from our calculations that the melt-front penetration for a sample with an amorphous layer 0.3 μm thick is somewhat greater

than can be accounted for solely by the increased absorption in the thicker layer. We suspect that this is a latent heat effect. There may be combinations of circumstances in which latent heat effects in an amorphous region are quite important, but we have not encountered such combinations in the annealing conditions we have assumed in our calculations.

#### D. Importance of carrier diffusion

As already mentioned, the calculations of Yoffa<sup>26</sup> seem to imply that the diffusion of the hot, dense gas of electrons and holes generated during laser annealing plays a dominant role in determining the temperature rise of the lattice. The following expression for the electron density in the near-surface region of a laser-irradiated sample is derived in Ref. 26,

$$N_{e,ss}(x) = \frac{g\hbar\omega_l\tau_e}{\hbar\omega} \frac{\delta/\alpha}{1 - (\delta/\alpha)^2} [e^{-x/\alpha} - (\delta/\alpha)e^{-x/\delta}]. \quad (9)$$

In this expression,  $g$  is the carrier generation rate,  $\delta$  is the absorption length ( $=1/k$ ) for laser radiation of frequency  $\omega_l$ ,  $\tau_e$  is the phonon-emission time due to collisions of the photoexcited electrons with the lattice, and  $\hbar\omega$  is the energy of the emitted phonons. The parameter  $\alpha$ , the characteristic diffusion length of the carriers, is discussed at length by Yoffa.

Equation (9) has a form analogous to

$$I(x) = (1 - R)I_0 k e^{-kx}, \quad (10)$$

which can be obtained from Eq. (6) when  $k$  is constant and the reflectivity factor  $1 - R$  is included. In Eq. (9),  $g\hbar\omega_l$  is the rate at which the incident radiation is absorbed in the sample by electronic excitations, and is therefore equivalent to  $(1 - R)I_0 k$  in Eq. (10). The quantity  $N_{e,ss}(x)(\hbar\omega/\tau_e)$  from Eq. (9) can be interpreted as the rate at

TABLE IV. Subsidiary computer data from the calculations designed to show the effects of the thermal properties of an amorphous region. The symbols are explained in the text.

Curve	$L_a/L_c$	$t_{m1}$ (nsec)	$E_{m1}$ (J/cm <sup>2</sup> )	$t_{m2}$ (nsec)	$E_{m2}$ (J/cm <sup>2</sup> )	$E_{at}$ (J/cm <sup>2</sup> )	$d_{max}$ (μm)	$T_{max}$ (°C)
(Fig. 5)								
—■—	1.0	18.0	0.210	23.2	0.350	0.635	0.453	1723
—▲—	1.0	16.4	0.176	22.0	0.316	0.622	0.510	2049
-----	1.0	17.9	0.209	21.2	0.292	0.613	0.463	1718
—●—	1.0	14.6	0.139	17.1	0.191	0.574	0.411	1660
(Fig. 6)								
a	0.6	10.1	0.182	11.4	0.232	0.646	0.333	1871
b	1.0	10.1	0.182	12.2	0.265	0.658	0.310	1809
c	0.6	49.9	0.333	53.5	0.383	0.739	0.205	1489
d	1.0	49.9	0.333	55.7	0.416	0.752	0.175	1468

which the absorbed energy is given up to the lattice through electron-lattice interactions and is equivalent to  $I(x)$  in Eq. (10). Equation (9) can thus be rewritten as

$$I(x) = (1-R)I_0(\alpha - \delta)^{-1}(\alpha + \delta)^{-1}(\alpha e^{-x/\alpha} - \delta e^{-x/\delta}). \quad (11)$$

If carrier diffusion is negligible,  $\alpha = 0$ , and Eq. (11) reduces to Eq. (10) as it should.

In an illustrative calculation, Yoffa chose  $\hbar\omega_i = 2.3$  eV,  $\delta = 10^{-5}$  cm,  $R = 0.5$ , and a typical annealing pulse of  $10^8$  W/cm<sup>2</sup>. This choice corresponds approximately to a 1.5-J/cm<sup>2</sup>, 15-nsec square pulse of a frequency-doubled Nd:YAG laser and leads to an estimate for  $\alpha$  of  $2.5 \times 10^{-5}$  cm. Figure 14 shows the ratio  $F_{\text{abs}} \equiv I(x)/(1-R)I_0$  as a function of  $x$  for four different sets of values for  $\alpha$  and  $\delta$ . The very high value of  $k = 1/\delta = 10^5$  cm<sup>-1</sup> assumed by Yoffa does indeed make the effects of carrier diffusion appear to be significant (compare ● with ▲). However, from the figure it is seen that the ▲ curve is approximated very well by the ○ curve, which is obtained by using an effective absorption coefficient of  $k = (1.0 + 2.5)^{-1} \times 10^5$  cm<sup>-1</sup> =  $2.86 \times 10^4$  cm<sup>-1</sup> in the simple exponential form of Eq. (10) or  $\delta = 3.5 \times 10^{-5}$  cm,  $\alpha = 0$  in Eq. (11).

From results of calculations of melt-front penetration as a function of absorption coefficient on Fig. 10, it can be seen that the maximum penetration depth of the melt front in the  $c$  model is essentially constant for wide ranges of the effective absorption coefficient. In fact, the four curves on Fig. 14 give very similar melt-front behavior. Hence, within certain limits, it does not really matter with this model whether or not carrier diffusion of the magnitude estimated by Yoffa is present. The results for the  $a$  model are more

sensitive to values of  $k_d$  for an obvious reason. With an amorphous layer only 0.15  $\mu\text{m}$  thick, much of the absorption of the laser radiation may occur in the crystalline region where  $k$  is assumed to be only  $3 \times 10^3$  cm<sup>-1</sup> (a value which is almost certainly too low, see Sec. IVI). As  $k_d$  increases, the percentage of the radiation absorbed in the 0.15- $\mu\text{m}$  layer increases rapidly also, leading to the dashed curve on Fig. 10. Nevertheless, even for this model much larger values of  $\alpha$  than those estimated by Yoffa would be required to reduce the effective absorption coefficient to the extent that the essential predictions of the melting model of pulsed-laser annealing would be made invalid.

On the other hand, there are certainly circumstances in which carrier diffusion should be important. These are most likely to occur in silicon for very short, intense pulses of high-frequency radiation. In such cases, carrier diffusion may have the beneficial effect of delaying the onset of surface vaporization. We suspect that carrier diffusion will be much more important in direct band-gap semiconductors such as GaAs than it is in Si. Earlier work of Blinov *et al.* (Ref. 9) seems to bear this out.

## VI. CONCLUSIONS

Calculations of the type presented in this paper evidently provide a great deal of information about the pulsed-laser annealing process. However, it is primarily after this information is used in calculations of dopant diffusion that extensive comparisons between experiment and theory can be made. Such comparisons will be made in the next paper of this series and it will be seen that excellent agreement between experimental and calculated dopant profiles is obtained for a variety of experiments. Also, as we have

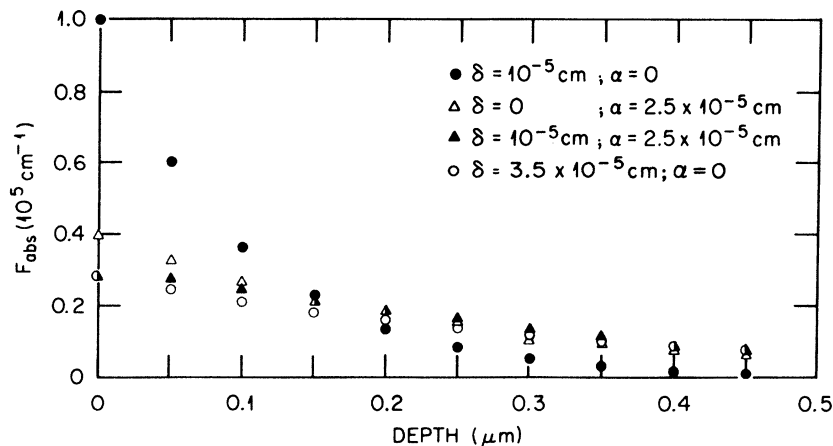


FIG. 14. The ratio  $F_{\text{abs}} \equiv [I(x)/(1-R)I_0]$  of Eq. (11) as a function of distance from the front surface of the sample.

seen from Fig. 13, the agreement between measured and calculated duration of surface melting is quite satisfactory. We conclude, therefore, that at this time there is no compelling reason to question the basic validity of the melting model of pulsed-laser annealing, although plasma effects may indeed play a minor role. The development of new experimental techniques and improvements

in existing ones should lead to further refinement of the model and of calculations based on it.

Research was sponsored by the Division of Materials Sciences, U.S. Department of Energy under Contract No. W-7405-eng-26 with the Union Carbide Corporation.

- <sup>1</sup>J. C. Wang, R. F. Wood, and P. P. Pronko, *Appl. Phys. Lett.* **33**, 455 (1978).
- <sup>2</sup>J. C. Wang, R. F. Wood, C. W. White, B. R. Appleton, P. P. Pronko, S. R. Wilson, and W. H. Christie, in *Laser-Solid Interactions and Laser Processing—1978*, Materials Research Society, Boston, Proceedings of the Symposium on Laser-Solid Interactions and Laser Processing, edited by S. D. Ferris, H. J. Leamy, and J. M. Poate (American Institute of Physics, New York, 1979).
- <sup>3</sup>R. F. Wood, G. E. Giles, and J. R. Kirkpatrick, in *Laser Applications in Materials Processing*, edited by J. F. Ready (Society of Photo-Optical Instrumentation Engineers, Bellingham, Washington, 1980), Vol. 198, p. 2.
- <sup>4</sup>R. F. Wood, J. C. Wang, G. E. Giles, and J. R. Kirkpatrick, in *Laser and Electron Beam Processing of Materials*, edited by C. W. White and P. S. Peercy (Academic, New York, 1980), p. 37.
- <sup>5</sup>J. R. Kirkpatrick, G. E. Giles, Jr., and R. F. Wood, paper No. AIAA-80-1473 (American Institute of Aeronautics, New York).
- <sup>6</sup>G. E. Giles, J. R. Kirkpatrick, and R. F. Wood, paper No. 80-HT-13, American Society of Mechanical Engineers, New York.
- <sup>7</sup>J. Narayan, R. T. Young, R. F. Wood, and W. H. Christie, *Appl. Phys. Lett.* **33**, 338 (1978).
- <sup>8</sup>R. T. Young, J. Narayan, and R. F. Wood, *Appl. Phys. Lett.* **35**, 447 (1979).
- <sup>9</sup>L. M. Blinov, V. S. Vavilov, and G. N. Galkin, *Fiz. Tekh. Poluprovodn.* **1**, 1351 (1967) [*Sov. Phys.—Semicond.* **1**, 1124 (1967)].
- <sup>10</sup>K. G. Svantesson, N. G. Nilsson, and L. Hult, *Solid State Commun.* **9**, 213 (1971).
- <sup>11</sup>I. B. Khaibullin, E. I. Shtyrkov, M. M. Zaripov, M. R. Galyautdinov, and G. G. Zakirov, *Fiz. Tekh. Poluprovodn.* **11**, 330 (1977) [*Sov. Phys.—Semicond.* **11**, 190 (1977)].
- <sup>12</sup>I. B. Khaibullin, E. I. Shtyrkov, M. M. Zaripov, R. M. Bayazitov, and M. F. Galyautdinov, *Radiat. Eff.* **36**, 225 (1978).
- <sup>13</sup>P. Baeri, S. U. Campisano, G. Foti, and E. Rimini, *Appl. Phys. Lett.* **33**, 137 (1978); *J. Appl. Phys.* **50**, 788 (1979).
- <sup>14</sup>D. H. Auston, C. M. Surko, T. N. C. Venkatesan, R. E. Slusher, and J. A. Golovchenko, *Appl. Phys. Lett.* **33**, 437 (1978).
- <sup>15</sup>H. W. Lo and A. Compaan [*Phys. Rev. Lett.* **44**, 1604 (1980)] have interpreted their results on pulsed Raman scattering during laser annealing of silicon to imply that the sample does not melt. We believe that these experiments are too preliminary and subject to too many uncertainties to warrant this conclusion at this time.
- <sup>16</sup>J. A. van Vechtan, in *Laser and Electron Beam Processing of Materials*, edited by C. W. White and P. S. Peercy (Academic, New York, 1980), p. 53.
- <sup>17</sup>W. D. Turner, D. C. Elrod, and I. I. Siman-Tov, *HEATING5—An IBM 360 Heat Conduction Program*, ORNL/CSD/TM-15 (Oak Ridge National Laboratory, Oak Ridge, Tennessee, 1977).
- <sup>18</sup>In practice, any laser beam will have some spatial inhomogeneities in it and these will destroy the one-dimensional character of the problem in localized regions. Control of these inhomogeneities is one of the problems which must be solved or circumvented in applications of laser annealing.
- <sup>19</sup>A. Goldsmith, T. E. Waterman, and H. J. Hirschhorn, *Handbook of Thermophysical Properties of Solid Materials* (Pergamon, New York, 1961), Vol. 1, p. I-576.
- <sup>20</sup>See for example C. J. Glassbrenner and G. A. Slack, *Phys. Rev.* **134**, A1058 (1964) and references therein.
- <sup>21</sup>The electrical conductivity of molten silicon was taken from V. M. Glasov, S. N. Chizhevskaya, and N. N. Glagoleva, *Liquid Semiconductors* (Plenum, New York, 1969), Chap. 3.
- <sup>22</sup>K. M. Shvarev, B. A. Baum, and P. V. Gel'd, *Fiz. Tverd. Tela (Leningrad)* **16**, 3246 (1974) [*Sov. Phys.—Solid State* **16**, 2111 (1975)].
- <sup>23</sup>A. A. Grinberg, R. F. Mekhtiev, S. M. Ryvkin, V. M. Salmanov, and I. D. Yaroshetskii, *Fiz. Tverd. Tela (Leningrad)* **9**, 1390 (1967) [*Sov. Phys.—Solid State* **9**, 1085 (1967)].
- <sup>24</sup>W. C. Dash and R. Newman, *Phys. Rev.* **99**, 1151 (1955).
- <sup>25</sup>M. H. Brodsky, R. S. Title, K. Weiser, and G. D. Petit, *Phys. Rev. B* **1**, 2632 (1970).
- <sup>26</sup>E. J. Yoffa, *Appl. Phys. Lett.* **36**, 37 (1980); *Phys. Rev. B* **21**, 2415 (1980).
- <sup>27</sup>Discussions of most of the numerical techniques mentioned in this subsection can be found in R. D. Richtmyer and K. W. Morton, *Difference Methods for Initial Value Problems*, 2nd ed. (Interscience, New York, 1967). See also S. Levy, Use of "Explicit Method" in Heat Transfer Calculations with an Arbitrary Time Step, General Electric Report No. 68-C-282, New York (unpublished).
- <sup>28</sup>See for example, C. Kittel, in *Introduction to Solid State Physics*, 3rd ed. (Wiley, New York, 1967), p. 193.
- <sup>29</sup>C. M. Surko, A. L. Simons, D. H. Auston, J. A.

- Golovchenko, R. E. Slusher, and T. N. C. Venkatesan, *Appl. Phys. Lett.* **34**, 635 (1979); D. H. Auston, J. A. Golovchenko, A. L. Simons, R. E. Slusher, P. R. Smith, C. M. Surko, and T. N. C. Venkatesan, in *Laser-Solid Interactions and Laser Processing—1978*, Materials Research Society, Boston, Proceedings of the Symposium on Laser-Solid Interactions and Laser Processing, edited by S. D. Ferris, H. J. Leamy, and J. M. Poate (American Institute of Physics, New York, 1979).
- <sup>30</sup>See for example, K. A. Jackson, *Can. J. Phys.* **36**, 683 (1958), and C. D. Thurmond, in *Semiconductors*, edited by N. B. Hannay (Reinhold, New York, 1959), p. 145.
- <sup>31</sup>G. J. van Gurp, G. E. Eggermont, Y. Tamminga, W. T. Stacy, and J. R. M. Gijbers, *Appl. Phys. Lett.* **35**, 273 (1979).
- <sup>32</sup>J. Narayan, *J. Metals* **32**, 15 (1980).
- <sup>33</sup>W. W. Mullins and R. F. Sekerka, *J. Appl. Phys.* **35**, 444 (1964).
- <sup>34</sup>F. A. Trumbore, *Bell System Tech. J.* **39**, 205 (1960).
- <sup>35</sup>See for example, V. G. Smith, W. A. Tiller, and J. W. Rutter, *Can. J. Phys.* **33**, 723 (1955).
- <sup>36</sup>C. W. White, J. Narayan, and R. T. Young, *Science* **204**, 461 (1979).
- <sup>37</sup>C. W. White, S. R. Wilson, and B. R. Appleton, *J. Appl. Phys.* **51**, 738 (1980).
- <sup>38</sup>R. F. Wood, *Appl. Phys. Lett.* **37**, 302 (1980).